

Time like geodesics in three-dimensional rotating Hořava AdS black hole

P. A. González*

*Facultad de Ingeniería y Ciencias, Universidad Diego Portales,
Avenida Ejército Libertador 441, Casilla 298-V, Santiago, Chile.*

Marco Olivares†

*Facultad de Ingeniería y Ciencias, Universidad Diego Portales,
Avenida Ejército Libertador 441, Casilla 298-V, Santiago, Chile.*

Eleftherios Papantonopoulos‡

Department of Physics, National Technical University of Athens, Zografou Campus GR 157 73, Athens, Greece.

Yerko Vásquez§

*Departamento de Física, Facultad de Ciencias,
Universidad de La Serena,
Avenida Cisternas 1200, La Serena, Chile.*

(Dated: April 1, 2021)

We study the motion of particles in the background of a three-dimensional rotating Hořava AdS black hole that corresponds to a Lorentz-violating version of the BTZ black hole and we analyze the effect of the breaking of Lorentz invariance in such motion by solving analytically the geodesic equations. Mainly, we find that Lorentz-violating version of the BTZ black hole posses a more rich geodesic structure, where the planetary and circular orbits are allowed, which does not occurs in the BTZ background.

PACS numbers:

Keywords:

Contents

I. Introduction	2
II. Three-dimensional rotating Hořava black holes	2
III. Equations of motion	5
IV. Time like geodesics	6
A. Planetary orbit	8
B. Circular orbits	11
C. Critical trajectories	15
D. Motion with $L = 0$	18
V. Remarks and conclusions	19
Acknowledgments	20
References	20

*Electronic address: pablo.gonzalez@udp.cl

†Electronic address: marco.olivares@mail.udp.cl

‡Electronic address: lpapa@central.ntua.gr

§Electronic address: yvasquez@userena.cl

I. INTRODUCTION

The three-dimensional models of gravity are of interest because it is possible to investigate efficiently some of their properties which are shared by their higher dimensional analogs, and also exhibit interesting solutions such as particle-like solutions and black holes. In this context, three-dimensional general relativity (GR), which has no local gravitational degrees of freedom, and is Lorentz invariant presents the well know Bañados–Teitelboim–Zanelli (BTZ) black hole solution with a negative cosmological constant [1]. Also, it presents interesting properties at both classical and quantum levels and the BTZ solution shares several features of the Kerr black hole [2]. An important issue in gravitational physics is to know the kind of orbits that test particles follow outside the event horizon of a black hole. This information can be provided by studying the geodesics around these black holes, in this context for the BTZ background it was shown that while massive particles always fall into the event horizon and no stable orbits are possible [3], massless particles can escape or plunge to the horizon [4].

The three-dimensional Hořava gravity [5] admits a Lorentz-violating version of the BTZ black hole, i.e. a black hole solution with AdS asymptotics, only in the sector of the theory in which the scalar degree of freedom propagates infinitely fast [6]. Remarkably, in contrast to GR, the three-dimensional Hořava gravity also admits black holes with positive and vanishing cosmological constant. Nowadays, one could think that Lorentz invariance may not be fundamental or exact, but is merely an emergent symmetry on sufficiently large distances or low energies. It has been suggested in Ref. [7] that giving up Lorentz invariance by introducing a preferred foliation and terms that contain higher-order spatial derivatives can lead to significantly improved UV behavior, the corresponding gravity theory is dubbed Hořava gravity. It was shown that the propagation of massive scalar fields is stable in the background of rotating three-dimensional Hořava AdS black holes and by employing the holographic principle the different relaxation times of the perturbed system to reach thermal equilibrium were found for the various branches of solutions [8]. Also, concerning to the collision of particles, it was shown that the particles can collide on the inner horizon with arbitrarily high CM energy if one of the particles has a critical angular momentum being possible the BSW process, for the non-extremal rotating Hořava AdS black hole. Also, while that for the extremal BTZ black hole the particles with critical angular momentum only can exist on the degenerate horizon, for the Lorentz-violating version of the BTZ black hole the particle with critical angular momentum can exist in a region from the degenerate horizon [9]. Concerning to the null geodesics, it was shown that for the motion of photons new kinds of orbits are allowed, such as unstable circular orbits and trajectories of first kind. Also, it was shown that an external observer will see that photons arrive at spatial infinity in a finite coordinate time [10].

In this work we study the motion of particles in the background of a three-dimensional rotating Hořava AdS black hole [6], with the aim of analyzing the effect of breaking the Lorentz symmetry by calculating the time like geodesic structure. We will show that Lorentz-violating version of the BTZ black hole posses a more rich geodesic structure, where the planetary orbits are allowed, which does not occur in the BTZ background. Also, we will have a complete knowledge of the geodesic structure for the rotating three-dimensional Hořava AdS black hole allowing us to understand in depth the Lorentz-violating effects on the BTZ black hole. For other studies about geodesics in three-dimensional spacetimes, see [11–14].

The work is organized as follows. In Sec. II we give a brief review of three-dimensional rotating Hořava AdS black hole. In Sec. III we find the motion equations for particles and we present the time like geodesic structure in Sec. IV. Finally, our conclusions are in Sec. V.

II. THREE-DIMENSIONAL ROTATING HOŘAVA BLACK HOLES

The three-dimensional Hořava gravity is described in a preferred foliation by the action [5]

$$S_H = \frac{1}{16\pi G_H} \int dT d^2x N \sqrt{g} [L_2 + L_4], \quad (1)$$

being the line element in the preferred foliation

$$ds^2 = N^2 dT^2 - g_{ij}(dx^i + N^i dT)(dx^j + N^j dT), \quad (2)$$

where g_{ij} is the induced metric on the constant- T hypersurfaces. G_H is a coupling constant with dimensions of a length squared, g is the determinant of g_{ij} and the Lagrangian L_2 has the following form

$$L_2 = K_{ij}K^{ij} - \lambda K^2 + \xi \left({}^{(2)}R - 2\Lambda \right) + \eta a_i a^i, \quad (3)$$

where K_{ij} , K , and ${}^{(2)}R$ correspond to extrinsic, mean, and scalar curvature, respectively, and a_i is a parameter related to the lapse function N via $a_i = -\partial_i \ln N$. L_4 corresponds to the set of all the terms with four spatial derivatives that are invariant under diffeomorphisms. For $\lambda = \xi = 1$ and $\eta = 0$, the action reduces to that of general relativity. In the infrared limit of the theory the higher order terms L_4 (UV regime) can be neglected, and the theory is equivalent to a restricted version of the Einstein-aether theory, the equivalence can be showed by restricting the aether to be hypersurface-orthogonal and the following relation is obtained

$$u_\alpha = \frac{\partial_\alpha T}{\sqrt{g^{\mu\nu} \partial_\mu T \partial_\nu T}}, \quad (4)$$

where u_α is a unit-norm vector field called the aether, see Ref. [15] for details. Another important characteristic of this theory is that only in the sector $\eta = 0$, Hořava gravity admits asymptotically AdS solutions [6]. Therefore, assuming stationary and circular symmetry the most general metric is given by

$$ds^2 = Z(r)^2 dt^2 - \frac{1}{F(r)^2} dr^2 - r^2 (d\phi + \Omega(r) dt)^2, \quad (5)$$

and by assuming the aether to be hypersurface-orthogonal, it results

$$u_t = \pm \sqrt{Z(r)^2 (1 + F^2(r) U^2(r))}, u_r = U(r). \quad (6)$$

The theory admits the BTZ “analogue” to the three-dimensional rotating Hořava black holes described by the solution

$$F(r)^2 = Z(r)^2 = -M + \frac{\bar{J}^2}{4r^2} - \bar{\Lambda} r^2, \quad \Omega(r) = -\frac{J}{2r^2}, \quad U(r) = \frac{1}{F(r)} \left(\frac{a}{r} + br \right), \quad (7)$$

where

$$\bar{J}^2 = \frac{J^2 + 4a^2(1 - \xi)}{\xi}, \quad \bar{\Lambda} = \Lambda - \frac{b^2(2\lambda - \xi - 1)}{\xi}. \quad (8)$$

The sign of the effective cosmological constant $\bar{\Lambda}$ determines the asymptotic behavior (flat, dS, or AdS) of the metric. Also, \bar{J}^2 can be negative, this occurs when either $\xi < 0$ or $\xi > 1$, $a^2 > J^2/(4(\xi - 1))$. The aether configuration for this metric is given explicitly by

$$u_t = \sqrt{F^2 + \left(\frac{a}{r} + br \right)^2}, \quad u_r = \frac{1}{F^2} \left(\frac{a}{r} + br \right), \quad u_\phi = 0, \quad (9)$$

where a and b are constants that can be regarded as measures of aether misalignment, with b as a measure of asymptotically misalignment, such that for $b \neq 0$ the aether does not align with the timelike Killing vector asymptotically. Note that for $\xi = 1$ and $\lambda = 1$, the solution becomes the BTZ black hole, and for $\xi = 1$ and $\lambda \neq 1$, the solution becomes the BTZ black hole with a shifted cosmological constant $\bar{\Lambda} = \Lambda - 2b^2(\lambda - 1)$. However, there is still a preferred direction represented by the aether vector field which breaks Lorentz invariance for $\lambda \neq 1$ and $b \neq 0$. The locations of the inner and outer horizons $r = r_\pm$, are given by

$$r_\pm^2 = -\frac{M}{2\bar{\Lambda}} \left(1 \pm \sqrt{1 + \frac{\bar{J}^2 \bar{\Lambda}}{M^2}} \right). \quad (10)$$

Considering $M > 0$, a negative cosmological constant $\bar{\Lambda} < 0$, and $\bar{J}^2 > 0$ the condition $-\bar{J}^2 \bar{\Lambda} \leq M^2$ must be fulfilled for the solution represents a black hole. For $0 < -\bar{J}^2 \bar{\Lambda} < M^2$ the black holes have inner and outer horizons r_- and r_+ , the extremal case corresponds to $-\bar{J}^2 \bar{\Lambda} = M^2$, while that for $\bar{J}^2 < 0$ the black holes have outer horizon r_+ , but no inner horizon r_- .

Besides the existence of inner and outer horizons, also there are universal horizons, which are given by [6]

$$(r_u^\pm)^2 = \frac{M - 2ab}{2(b^2 - \bar{\Lambda})} \pm \frac{1}{2(b^2 - \bar{\Lambda})} \left[(M - 2ab)^2 - (4a^2 + \bar{J}^2)(b^2 - \bar{\Lambda}) \right]^{\frac{1}{2}}. \quad (11)$$

On the other hand, the existence of a well-defined spacelike foliation is essential in Hořava gravity. As, it was shown in Ref. [6], this can be achieved by imposing the condition $F^2 + (a/r + br)^2 > 0$ or

$$\frac{1}{r^2} \left((b^2 - \bar{\Lambda})r^4 + (2ab - M)r^2 + \left(\frac{\bar{J}}{4} + a^2 \right) \right) > 0. \quad (12)$$

The Fig. (1), show the behavior of the horizons as a function of the parameter b , and as a function of a in Fig. (2), for a choice of parameters. There are different zones, one of them is limited by r_- and r_+ ; and it is described by the existence of the aether, where the roots r_u^\pm are imaginary and therefore there are no universal horizons. Other zones are characterized by two real and distinct universal horizons inside the region between r_- and r_+ , outside r_- , and inside r_+ ; and an especial zone where both universal horizons coincide and is given by

$$r_u^2 = \frac{M - 2a_\pm(M, \bar{J}, b)b}{2(b^2 - \bar{\Lambda}(b))}, \quad (13)$$

where a_\pm are the roots of

$$\frac{(4a^2 + \bar{J}^2)(b^2 - \bar{\Lambda}(b))}{\xi(M - 2ab)^2} = 1. \quad (14)$$

In the region between r_u^- and r_u^+ , the aether turns imaginary and the foliation cannot be extended until the singularity.

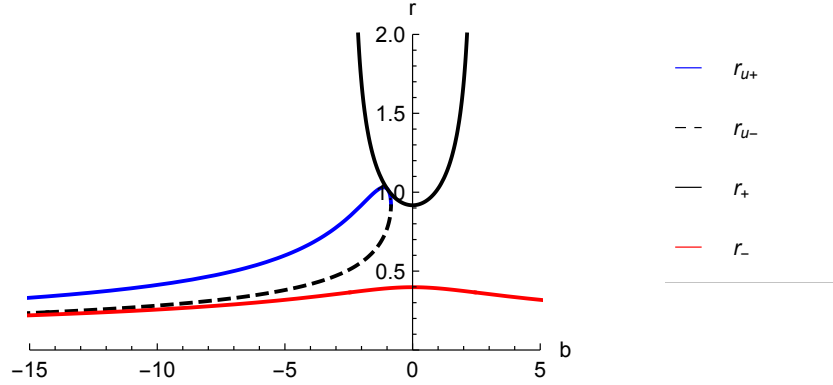


FIG. 1: The behavior of the horizons as a function of the parameter b , with $M = 1$, $\xi = 1.2$, $\lambda = 1$, $a = 1$, $\Lambda = -1$, and $J = 1.2$. For $b \approx -0.84$, $r_u^+ = r_u^-$ [9].

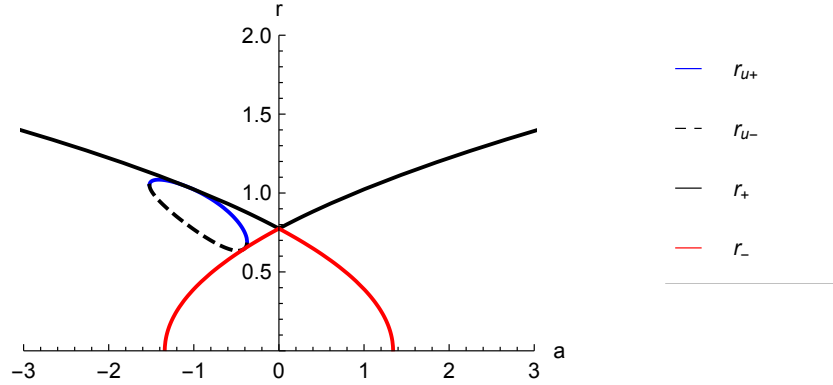


FIG. 2: The behavior of the horizons as a function of the parameter a , with $M = 1$, $\xi = 1.2$, $\lambda = 1$, $b = 1$, $\Lambda = -1$, and $J = 1.2$. For $a \approx -1.52$, and -0.37 , $r_u^+ = r_u^-$ [9].

In order to analysis the roots of the lapse function the case $J = 0$, we will consider a set of values for the parameters that satisfied the existence of two horizons r_- and r_+ , so the condition $0 < -\bar{J}^2\bar{\Lambda} < M^2$ must be satisfied, and also there are not universal horizons, thereby the roots of r_u^\pm are imaginary, as in our previous analysis. So, in order to satisfy the above condition the parameter ξ must satisfied $\xi_e < \xi < \xi_c$, where ξ_e corresponds to the value of ξ for which the black hole is extremal

$$\xi_e = \frac{2a^2 \left(\sqrt{a^2 (\Lambda - 2b^2(\lambda - 1))^2 + b^2(2\lambda - 1)M^2 - 2b^2\lambda - \Lambda} \right)}{M^2 - 4a^2(b^2 + \Lambda)}, \quad (15)$$

and ξ_c is the value of ξ for which the black hole passes from having two horizons to having one horizon and it is $\xi_c = 1$ for non-rotating black holes. For $\xi > \xi_c$ the black holes are described by one horizon [8]. In Fig. 3, we plot the behaviour of the horizons for $\xi = 0.9$ for non-rotating black holes.

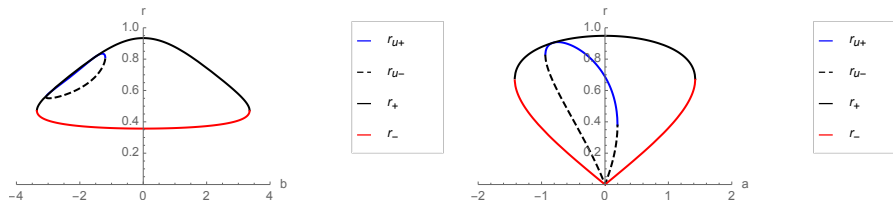


FIG. 3: The behavior of the horizons for non-rotating black holes as a function of the parameter b (left panel) with $a = 1$, and as a function of the parameter a (right panel) with $b = 1$. Here, $M = 1$, $\xi = 0.9$, $\lambda = 1$, and $\Lambda = -1$.

In the following we will focus mainly on a set of values for the parameters that satisfied the existence of two horizons r_- and r_+ , with $a > 0$, and $b > 0$, where there are not universal horizons, thereby the roots of r_u^\pm are imaginary, see Figs. 1, 2, and 3. Note that under the conditions $M > 0$, $\bar{J}^2 > 0$, and $\bar{\Lambda} < 0$, the roots of r_u^\pm are imaginary when $M < 2ab$ from Eq. (11).

III. EQUATIONS OF MOTION

In this section, we find the motion equations of probe massive particles around the three-dimensional Hořava AdS black hole. It is important to emphasize [16] that in a Lorentz-violating scenario, particles will be generically coupled to the aether field generating UV modifications of the matter dispersion relations, it is more, one can also expect radiative corrections in the infrared sector but these contributions are suppressed by known mechanisms. In our analysis we are interested on the infrared limit of the theory; so the presence of higher-order terms (L_4) related to the UV behaviour of the theory are ignored and in this case the theory can be formulated in a covariant fashion, and it then becomes equivalent to a restricted version of Einstein-aether theory [6]. Since our analysis is focused in the low energy part of the theory, the interaction between the massive particle and the aether field is ignored, thus the presence of aether field only affect the background spacetime geometry. It is worth mentioning that a similar analysis was performed in [17] where the authors analyzed the evolution of the photon around the static neutral and charged aether black holes using the Hamilton-Jacobi equation. Therefore, the massive particles follow the typical geodesics in such given black holes spacetime, that can be derived from the Lagrangian of a test particle, which is given by [18]

$$\mathcal{L} = \frac{1}{2} \left(g_{\mu\nu} \frac{dx^\mu}{d\tau} \frac{dx^\nu}{d\tau} \right). \quad (16)$$

So, for the three-dimensional rotating Hořava AdS black hole described by the metric (5), the Lagrangian associated with the motion of the test particles is given by

$$2\mathcal{L} = -[\mathcal{F}(r) - r^2\Omega^2(r)]\dot{t}^2 + 2r^2\Omega(r)\dot{t}\dot{\phi} + \frac{\dot{r}^2}{\mathcal{F}(r)} + r^2\dot{\phi}^2, \quad (17)$$

where $\dot{q} = dq/d\tau$, and τ is an affine parameter along the geodesic. Here, we have defined $F(r)^2 = Z(r)^2 = \mathcal{F}(r)$. Since the Lagrangian (17) is independent of the cyclic coordinates (t, ϕ) , then their conjugate momenta (Π_t, Π_ϕ) are conserved. Then, the equations of motion are obtained from $\dot{\Pi}_q - \frac{\partial \mathcal{L}}{\partial q} = 0$, and yield

$$\dot{\Pi}_t = 0, \quad \dot{\Pi}_r = -[\mathcal{F}'(r)/2 - r\Omega^2(r) - r^2\Omega'(r)]\dot{t}^2 - \frac{\mathcal{F}'(r)\dot{r}^2}{2\mathcal{F}^2(r)} + r\dot{\phi}^2, \quad \text{and} \quad \dot{\Pi}_\phi = 0, \quad (18)$$

where $\Pi_q = \partial \mathcal{L} / \partial \dot{q}$ are the conjugate momenta to the coordinate q , and are given by

$$\Pi_t = -[\mathcal{F}(r) - r^2\Omega^2(r)]\dot{t} + r^2\Omega(r)\dot{\phi} \equiv -E, \quad \Pi_r = \frac{\dot{r}}{\mathcal{F}(r)} \quad \text{and} \quad \Pi_\phi = r^2\Omega(r)\dot{t} + r^2\dot{\phi} \equiv L, \quad (19)$$

where E and L are integration constants associated to each of them. Therefore, the Hamiltonian is given by

$$\mathcal{H} = \Pi_t \dot{t} + \Pi_\phi \dot{\phi} + \Pi_r \dot{r} - \mathcal{L}. \quad (20)$$

Thus,

$$2\mathcal{H} = -E\dot{t} + L\dot{\phi} + \frac{\dot{r}}{\mathcal{F}(r)} \equiv -m^2. \quad (21)$$

where $m = 1$ for timelike geodesics or $m = 0$ for null geodesics. Therefore, we obtain

$$\dot{\phi} = -\frac{1}{(r^2 - r_+^2)(r^2 - r_-^2)\bar{\Lambda}} \left[\frac{EJ}{2} + L \left(-\bar{\Lambda}r^2 - M - \frac{J^2 - \bar{J}^2}{4r^2} \right) \right], \quad (22)$$

$$\dot{t} = -\frac{[Er^2 - JL/2]}{(r^2 - r_+^2)(r^2 - r_-^2)\bar{\Lambda}}, \quad (23)$$

$$r^2 = \left(E - \frac{JL}{2r^2} \right)^2 - \left(-M + \frac{\bar{J}^2}{4r^2} - \bar{\Lambda}r^2 \right) \left(m^2 + \frac{L^2}{r^2} \right) = (E - V_-)(E - V_+), \quad (24)$$

where $V_\pm(r)$ is the effective potential and it is given by

$$V_\pm(r) = \frac{JL}{2r^2} \pm \sqrt{\left(-M + \frac{\bar{J}^2}{4r^2} - \bar{\Lambda}r^2 \right) \left(m^2 + \frac{L^2}{r^2} \right)}. \quad (25)$$

Since the negative branches have no classical interpretation, they are associated with antiparticles in the framework of quantum field theory [19]. We choose the positive branch of the effective potential $V = V_+$. In the next section we will perform a general analysis of the equations of motion. Note that if $\dot{t} > 0$ for all $r > r_+$ the motion is forward in time outside the horizon, so from Eq. (23) for $\bar{\Lambda} < 0$ the following condition must be fulfilled

$$Er^2 - JL/2 > 0. \quad (26)$$

On the other hand, Eq. (22) can be rewritten as

$$\dot{\phi} = -\frac{1}{(r^2 - r_+^2)(r^2 - r_-^2)\bar{\Lambda}} \left[\frac{J}{2r^2} \left(Er^2 - \frac{JL}{2} \right) + LF(r)^2 \right], \quad (27)$$

due to the term $Er^2 - JL/2 > 0$ and $F(r)^2 > 0$ for $r > r_+$, when L , and J have the same sign ($JL > 0$), the term in square-brackets have not zeros outside the event horizon. However, when L and J have different signs ($JL < 0$), the zeros can be in the relevant domain, and it would not necessarily indicate a turning point. In fact, the positive root (R) of the term in square-brackets in Eq. (22) is

$$R^2 = \frac{JE}{4\bar{\Lambda}L} - \frac{M}{2\bar{\Lambda}} - \frac{\sqrt{(4LM - 2JE)^2 - 16\bar{\Lambda}L(J^2L - \bar{J}^2L)}}{8\bar{\Lambda}L}, \quad (28)$$

and it corresponds to the point where the angular velocity of the test particle $\omega(r)$

$$\dot{\phi}/\dot{t} = \frac{d\phi}{dt} = \frac{\frac{EJ}{2} + L \left(-\bar{\Lambda}r^2 - M - \frac{J^2 - \bar{J}^2}{4r^2} \right)}{Er^2 - JL/2} \equiv \omega(r), \quad (29)$$

is null. Also, note that for a motion with $L = 0$, $\omega(r) = \frac{J}{2r^2}$. Thus, a particle dropped ‘straight in’ ($L = 0$) from a finite distance is ‘dragged’ just by the influence of gravity so that it acquires an angular velocity (ω) in the same sense as that of the source of the metric (J), effect called as “dragging of inertial frames”.

IV. TIME LIKE GEODESICS

In this section we analyze the motion of particles, $m^2 = 1$, so the effective potential is given by

$$V(r) = \frac{JL}{2r^2} + \sqrt{\left(-M + \frac{\bar{J}^2}{4r^2} - \bar{\Lambda}r^2 \right) \left(1 + \frac{L^2}{r^2} \right)}, \quad (30)$$

whose behaviour is showed in Fig. 4 for $J > 0$, and positive values of the angular momentum of the particle (direct geodesics), and for $J < 0$, and positive values of the angular momentum of the particle (retrograde geodesics). We can observe for direct geodesics (left panel), there is a critical value of the angular momentum (L_{LSCO}) where the last stable circular orbit (LSCO) is present at $r = r_{LSCO}$; and for $L > L_{LSCO}$ we can distinguish four orbits, the planetary, the second kind, the circular unstable at $r = r_U$, the circular stable at $r = r_S$, and critical orbits are allowed. We will study the existence of circular orbit in detail in subsection B. Note that, in the BTZ background is allowed orbits of second kind. So, the spacetime analyzed present a richer geodesic structure. Also, for retrograde geodesics (right panel) we can observe that, for $r > r_+$, circular and planetary orbits are not allowed. Here, the trajectory always have a turning point, from which the particle plunge in the event horizon, knowing as trajectory of second kind.

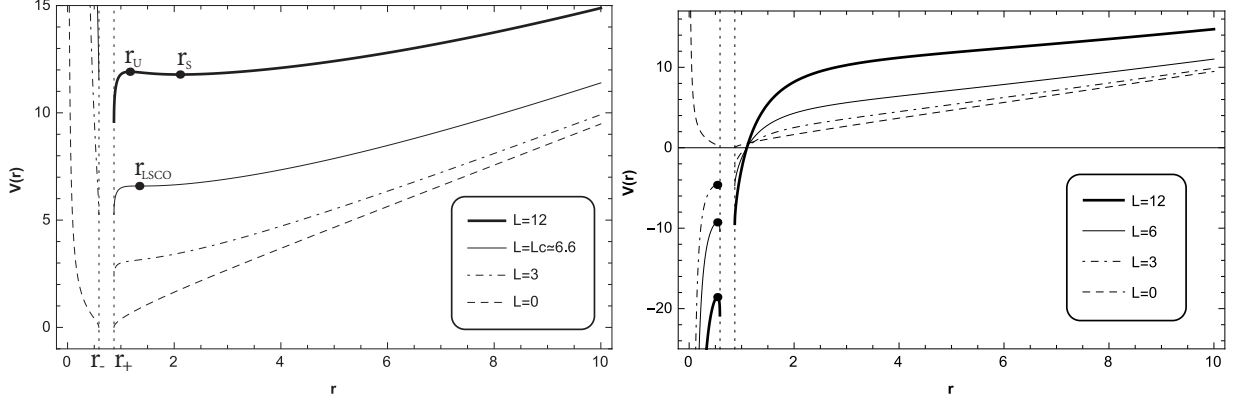


FIG. 4: The behavior of $V(r)$ as a function of r , for different values of the angular momentum of the particle L , with $M = a = b = \lambda = 1$, $\xi = 1.1$, $r_+ \approx 0.87$ and $\Lambda = -1$. Left panel for direct geodesics with $J = 1.2$, and right panel for retrograde geodesics with $J = -1.2$. The points (right panel) indicate the extreme value of the potential that are located at $r_{ext} < r_+$.

The orbit in polar coordinates is given by [21]

$$-\frac{r^2}{(r^2 - r_+^2)(r^2 - r_-^2)\bar{\Lambda}} \left[\frac{EJ}{2} + L \left(-\bar{\Lambda}r^2 - M - \frac{J^2 - \bar{J}^2}{4r^2} \right) \right] \left(\pm \frac{dr}{d\phi} \right) = \sqrt{P(r)}. \quad (31)$$

where we have used Eq. (22) and Eq. (24), $P(r)$ corresponds to the characteristic polynomial, and it is given by

$$P(r) = r^6 \bar{\Lambda} + r^4 (E^2 + L^2 \bar{\Lambda} + M) + r^2 (L^2 M - JEL - \bar{J}^2/4) + (J^2 - \bar{J}^2)L^2/4 \\ P(r) \equiv -\bar{\Lambda} (-r^6 + \alpha r^4 + \beta r^2 + \gamma). \quad (32)$$

where

$$\alpha = -\frac{E^2 + M + \bar{\Lambda}L^2}{\bar{\Lambda}}, \quad (33)$$

$$\beta = \frac{JEL + \bar{J}^2/4 - ML^2}{\bar{\Lambda}}, \quad (34)$$

$$\gamma = -\frac{(J^2 - \bar{J}^2)L^2}{4\bar{\Lambda}}, \quad (35)$$

Therefore, we can see that depending on the nature of its roots, we can obtain the allowed motions for this spacetime.

A. Planetary orbit

The roots of $P(r) = 0$ allows to define the distance r_P , which corresponds to a *periastron* distance at the trajectory, r_A which is interpreted as a *apoastron* distance, and the distance r_F that represent the turning point for the trajectory, see Fig. 5. Thereby, planetary orbits of the first kind occur when $L > L_C$, and the energy E lies in the range $E_S < E < E_U$, so the radial coordinate will be $r_p < r < r_A$ for a certain value of E ; and the planetary orbits of the second kind occurs when $E < E_U$, and $r_H < r < r_F$.

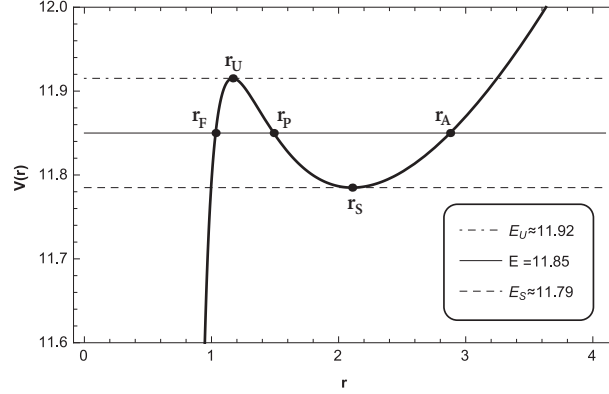


FIG. 5: The behavior of $V(r)$ as a function of r , for $L = 12$, $M = a = b = \lambda = 1$, $J = 1.2$, $\xi = 1.1$, $r_F \approx 1.03$, $r_U \approx 1.17$, $r_P \approx 1.49$, $r_S \approx 2.11$, $r_A \approx 2.88$, $E = 11.85$, $E_S = 11.79$, $E_U = 11.92$, and $\Lambda = -1$.

Thus, the characteristic polynomial (32) can be written as

$$P(r) = -\bar{\Lambda} (r_A^2 - r^2) (r^2 - r_P^2) (r^2 - r_F^2), \quad (36)$$

where

$$r_A = \left(\frac{\alpha}{3} + 2\sqrt{\frac{A}{3}} \cos \left[\frac{1}{3} \cos^{-1} \left[\frac{3B}{2} \sqrt{\frac{3}{A^3}} \right] \right] \right)^{1/2}, \quad (37)$$

$$r_P = \left(\frac{\alpha}{3} + 2\sqrt{\frac{A}{3}} \cos \left[\frac{1}{3} \cos^{-1} \left[\frac{3B}{2} \sqrt{\frac{3}{A^3}} \right] + \frac{4\pi}{3} \right] \right)^{1/2} \quad (38)$$

and

$$r_F = \left(\frac{\alpha}{3} + 2\sqrt{\frac{A}{3}} \cos \left[\frac{1}{3} \cos^{-1} \left[\frac{3B}{2} \sqrt{\frac{3}{A^3}} \right] + \frac{2\pi}{3} \right] \right)^{1/2} \quad (39)$$

where $A = \frac{\alpha^2}{3} + \beta$ and $B = \frac{2\alpha^3}{27} + \frac{\alpha\beta}{3} + \gamma$. Now, we will determine the angular coordinate of the trajectory for a particle that start at $r = r_A$, and it is given by the solution of the integral

$$\phi(r) = - \int_{r_A}^r \frac{r^2}{(-\bar{\Lambda})(r^2 - r_+^2)(r^2 - r_-^2)} \left[-L\bar{\Lambda}r^2 + \left(\frac{EJ}{2} - ML \right) - L \frac{J^2 - \bar{J}^2}{4r^2} \right] \frac{dr}{\sqrt{P(r)}}, \quad (40)$$

where we have used Eqs. (22) and (24), and whose solution is

$$\phi(r) = k_0 \Psi_0(r) + K_0 [k_+ \Psi_+(r) - k_- \Psi_-(r)], \quad (41)$$

where

$$k_0 = \frac{r_A L (J^2 - \bar{J}^2)}{8(-\bar{\Lambda})^{3/2} \sqrt{\gamma} r_+^2 r_-^2}, \quad \Psi_0(r) = \wp^{-1} [U(r_A)] - \wp^{-1} [U(r)], \quad (42)$$

$$k_{\pm} = \frac{EJ/2 - LM}{r_{\pm}^2} - \bar{\Lambda}L - \frac{L(J^2 - \bar{J}^2)}{4r_{\pm}^4}. \quad (43)$$

This solution is plotted in Fig. 6 for direct orbits, where we can observe the trajectory of first and second kind. Note that, the coordinate (ϕ) diverges at the event horizon. Also, the solution (41) allow us to determine the precession angle, by considering that it is given by $\Theta = 2\phi_P - 2\pi$, where ϕ_P is the angle from the apoastron to the periastron. Thus, we obtain

$$\Theta = 2k_0 \Psi_0(r_P) + 2K_0 [k_+ \Psi_+(r_P) - k_- \Psi_-(r_P)] - 2\pi. \quad (44)$$

This is an exact solution for the angle of precession, and it depends on the spacetime parameters; M , J , \bar{J} , and the particles motion constants, E and L .

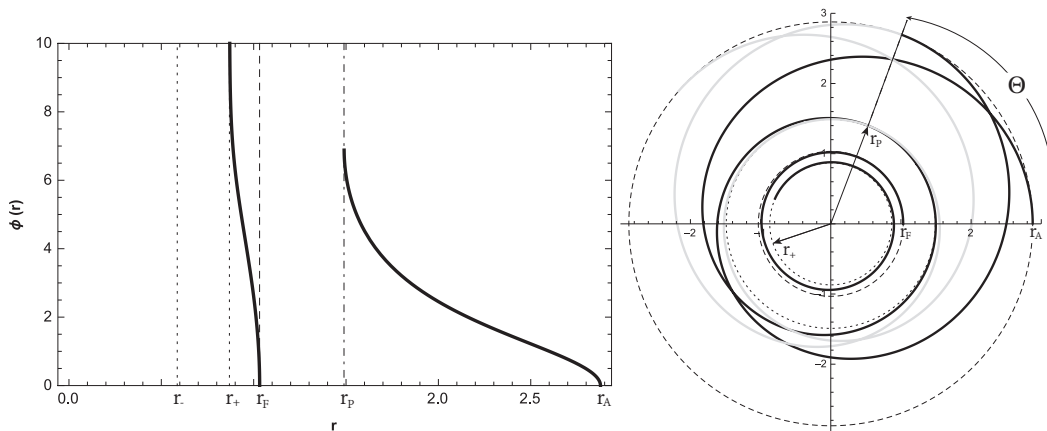


FIG. 6: Direct orbits. The behaviour of $\phi(r)$ (left panel), and $r(\phi)$ (right panel) for bounded orbits of first and second kind with $E = 11.85$, $L = 12$, $M = a = b = \lambda = 1$, $\Lambda = -1$, $J = 1.2$, and $\xi = 1.1$.

In Fig. 7, we plot the behaviour of the retrograde orbits, clearly they corresponds to second kind trajectories. Here, we can observe the effect of "dragging of inertial frames". The test particle start at $r = r_A$, then at $r = R$ the angular velocity is null, and $\phi(r)$ is maximum, after that the angle $\phi(r)$ decreases and tends to $-\infty$, when $r \rightarrow r_+$.

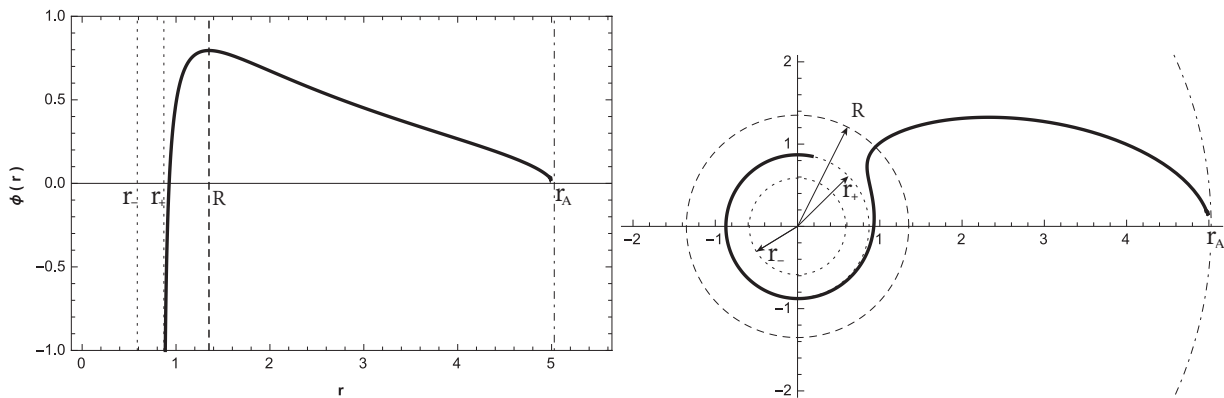


FIG. 7: Retrograde orbits. The behaviour of $\phi(r)$ (left panel), and $r(\phi)$ (right panel) for bounded orbits of second kind with $E = 11.85$, $L = 12$, $M = a = b = \lambda = 1$, $\Lambda = -1$, $J = -1.2$, $R = 1.35$, and $\xi = 1.1$.

Now, in order to determine the proper and coordinate period of rotation of the trajectories we present the solution for both times. The proper time (τ), is given by the solution of the integral

$$\tau(r) = - \int_{r_A}^r \frac{r^2 dr}{\sqrt{P(r)}}, \quad (45)$$

where we have used Eq. (24) and we have considered as initial conditions that the particles are at $r = r_A$ when $\phi = t = \tau = 0$. Thus, we obtain

$$\tau(r) = \frac{r_A^3}{8\sqrt{(-\Lambda)\gamma}} (\Psi[U(r), \Omega] - \Psi[U(r_A), \Omega]) , \quad (46)$$

where

$$\Psi(U, \Omega) = \frac{1}{\wp'(\Omega)} \left[2\zeta(\Omega)\wp^{-1}(U) + \ln \left| \frac{\sigma[\wp^{-1}(U) - \Omega]}{\sigma[\wp^{-1}(U) + \Omega]} \right| \right] , \quad (47)$$

and

$$U(r) = \frac{r_A^2}{4r^2} + \frac{\beta r_A^2}{12\gamma} , \quad U(r_A) = \frac{1}{4} + \frac{\beta r_A^2}{12\gamma} , \quad (48)$$

$$\Omega = \wp^{-1} \left[\frac{\beta r_A^2}{12\gamma} \right] , \quad (49)$$

$$g_2 = \frac{r_A^4}{4} \left[\frac{\beta^2}{3\gamma^2} - \frac{\alpha}{\gamma} \right] , \quad g_3 = \frac{r_A^6}{16} \left[\frac{\alpha\beta}{3\gamma^2} - \frac{2\beta^3}{27\gamma^3} + \frac{1}{\gamma} \right] . \quad (50)$$

In Fig. 8, we show the behaviour of the proper time as a function of r for direct orbits (left panel), we can observe, for the trajectory of first and second kind the particle arrives in a finite proper time to r_P , and to reach the singularity, respectively. Also, the period of a revolution according to the proper time is $T_\tau = 2\tau(r_P)$. Concerning to the retrograde orbits (right panel), for the trajectory of second kind the particle arrives in a finite proper time to the singularity.

On the other hand, by considering Eqs. (23) and (24), and as initial condition that the particles are at $r = r_A$ when $\phi = t = \tau = 0$. The coordinate time (t) is

$$t(r) = - \int_{r_A}^r \frac{r^2 [Er^2 - JL/2]}{(-\bar{\Lambda})(r^2 - r_+^2)(r^2 - r_-^2) \sqrt{P(r)}} dr , \quad (51)$$

whose solution is

$$t(r) = K_0 \left[\left(E - \frac{JL}{2r_+^2} \right) \Psi_+(r) - \left(E - \frac{JL}{2r_-^2} \right) \Psi_-(r) \right] , \quad (52)$$

where $K_0 = \frac{r_A^3}{8(-\bar{\Lambda})^{3/2}\sqrt{\gamma}(r_+^2 - r_-^2)}$, and

$$\Psi_\pm(r) = \Psi[U(r_A), \Omega_\pm] - \Psi[U(r), \Omega_\pm] , \quad \Omega_\pm(r) = \wp^{-1} \left[\frac{r_A^2}{4r_\pm^2} + \frac{\beta r_A^2}{12\gamma} \right] . \quad (53)$$

Also, in Fig. 8, we show the behaviour of the coordinate time as a function of r . For direct orbits, we can observe, for the trajectory of first and second kind the particle arrives in a finite and infinity coordinate time to r_P , and r_+ , respectively. Also, the period of a revolution according to the coordinate time is $T_t = 2t(r_P)$. Concerning to the retrograde orbits (right panel), for the trajectory of second kind the particle arrives in an infinite coordinate time to r_+ . Also, we can observe that the zero located at R does not affect to the proper and coordinate times.

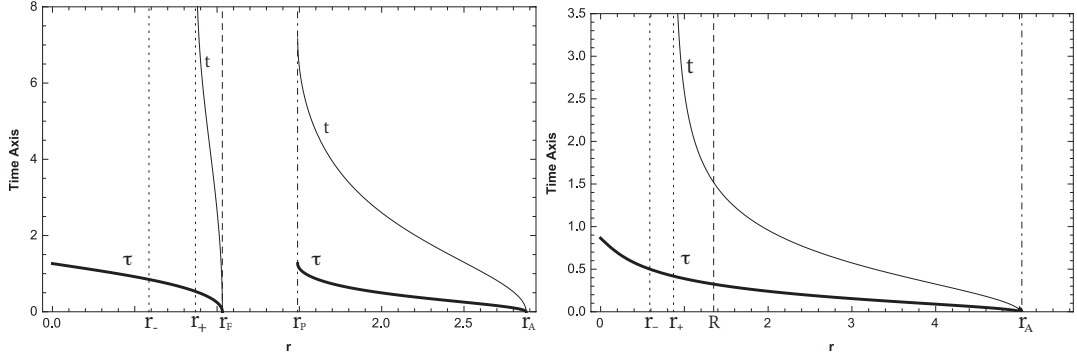


FIG. 8: The behaviour of the coordinate time (t) and the proper time (τ) along an bounded time-like geodesic described by a test particle, starting at r_A , and $r_F = 1.03$ with $r_P = 1.49$, $R = 1.35$, $L = 12$, $M = a = b = \lambda = 1$, $\Lambda = -1$, $E = 11.85$, $\xi = 1.1$, $r_+ \approx 0.87$, and $r_- \approx 0.59$. Left panel for direct orbits with $J = 1.2$, and $r_A = 2.88$, and right panel for retrograde orbits with $J = -1.2$, and $r_A = 5.03$.

B. Circular orbits

The effective potential $V(r)$ has to exhibit extrema for fixed values of radial coordinate, $r = r_{c.o.}$, when

$$\left. \frac{dV(r)}{dr} \right|_{r_{c.o.}} = 0. \quad (54)$$

Now, for simplicity, we write the effective potential as

$$V(r) = \frac{JL}{2r^2} + \sqrt{\mathcal{F}(r) + L^2 \frac{\mathcal{F}(r)}{r^2}}. \quad (55)$$

Therefore, using Eq. (55) into Eq. (54) yields

$$\left[r^3 \mathcal{F}'(r) + L^2 [r \mathcal{F}'(r) - 2\mathcal{F}(r)] - 2JL \sqrt{\mathcal{F}(r) + L^2 \frac{\mathcal{F}(r)}{r^2}} \right] \Big|_{r_{c.o.}} = 0. \quad (56)$$

Notice that this equation leads to a polynomial of twelfth grade given by,

$$\begin{aligned} & r_{c.o.}^{12} + \frac{\bar{J}^2 - 4L^2 M}{2\bar{\Lambda}} r_{c.o.}^8 + \frac{L^2 (J^2 + \bar{J}^2)}{\bar{\Lambda}} r_{c.o.}^6 + \\ & \frac{16J^2 L^2 (\bar{\Lambda} L^2 + M) + \bar{J}^2 (\bar{J}^2 - 8L^2 M) + 16L^4 M^2}{16\bar{\Lambda}^2} r_{c.o.}^4 + \\ & \frac{L^2 (J^2 - \bar{J}^2) (4L^2 M - \bar{J}^2)}{4\bar{\Lambda}^2} r_{c.o.}^2 - \frac{\bar{J}^2 L^4 (J^2 - \bar{J}^2)}{4\bar{\Lambda}^2} = 0, \end{aligned} \quad (57)$$

so, it is possible to find the roots numerically. On the other hand, the condition (56) allows to obtain the angular momentum for the stable $L_{c.o.} = L_S$ at $r_{c.o.} = r_S$ and for the unstable circular orbits $L_{c.o.} = L_U$ at $r_{c.o.} = r_U$, which yields

$$AL_{c.o.}^4 - BL_{c.o.}^2 + C = 0, \quad (58)$$

where

$$\begin{aligned} A &= \left[4(M^2 + \bar{\Lambda} J^2) + (J^2 - \bar{J}^2) \left(\frac{4M}{r^2} - \frac{\bar{J}^2}{r^4} \right) \right] \Big|_{r_{c.o.}}, \\ B &= \left[\frac{\bar{J}^2}{r^2} (J^2 - \bar{J}^2) - 2M(2J^2 - \bar{J}^2) - 4\bar{\Lambda} r^2 (J^2 + \bar{J}^2 - 2Mr^2) \right] \Big|_{r_{c.o.}}, \\ C &= \left[4\bar{\Lambda}^2 r^8 + 2\bar{\Lambda} \bar{J}^2 r^4 + \frac{\bar{J}^2}{4} \right] \Big|_{r_{c.o.}}. \end{aligned} \quad (59)$$

Thus, the real solution of the quartic equation for $L_{c.o.}$ is

$$L_{c.o.}^2 = \left[\frac{\mathcal{B} - \sqrt{\mathcal{B}^2 - 4\mathcal{A}\mathcal{C}}}{2\mathcal{A}} \right] \Big|_{r_{c.o.}}, \quad (60)$$

and the energy is given by $E_{c.o.} = JL_{c.o.}/2r_{c.o.}^2 + \sqrt{\mathcal{F}(r_{c.o.}) + L_{c.o.}^2 \mathcal{F}(r_{c.o.})/r_{c.o.}^2}$.

Now, in Fig. 9, we show the behaviour of the lapse function and the effective potential for different values of J . We can observe that J , can not take big values due to the spacetime became in a naked singularity, and for a very small value of J the black hole present only one event horizon, because the \bar{J}^2 became negative. So, only in spacetimes with sufficiently big $|J|$ do the circular co-rotating orbits in the domain $r > r_+$ exist.

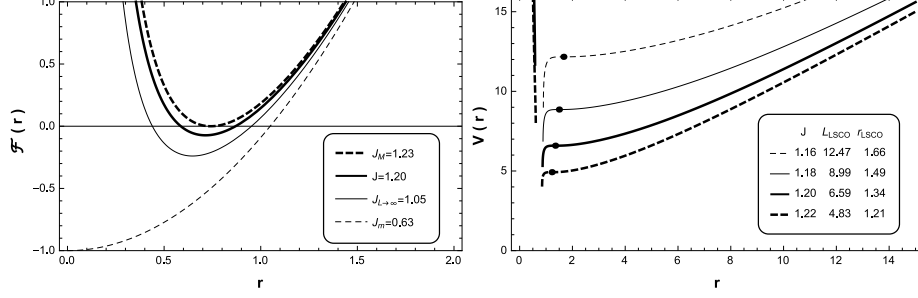


FIG. 9: The behaviour of the lapse function (left panel), and the behavior of $V(r)$ (right panel) as a function of r , for different values of the angular momentum of the black hole J , with $M = a = b = \lambda = 1$, $\xi = 1.1$, and $\Lambda = -1$. For $J = J_m = 2a\sqrt{\xi - 1}$ the black hole has one horizon at $r = r_+ = 1.05$, in the range $J_m < J < J_M$ the black hole has two horizons at $r = r_- = 0.40$, and $r = r_+ = 0.97$, and for $J = J_M = \sqrt{\frac{4a^2\bar{\Lambda}(\xi-1) - M^2\xi}{\bar{\Lambda}}}$ the black hole is extremal at $r = r_e = 0.74$. $J = J_{L \rightarrow \infty} = \sqrt{-M^2/\bar{\Lambda}}$ corresponds to the value of J for which the minimum radius of the stable circular orbit diverges, see Eq. (61).

Also, the behaviour of the effective potential for different values of angular momentum L , is shown in Fig. 10. We can observe that for $L > L_{LSCO}$, when the angular momentum increases the radius of the stable circular orbit increases, and the radius of the unstable circular orbit (r_U) decreases. Also, when $L \rightarrow \infty$ the $r_U \rightarrow R_U$, is given by

$$R_U = \left[\frac{-M(J^2 - \bar{J}^2) - |J|\sqrt{(J^2 - \bar{J}^2)(M^2 + \bar{\Lambda}\bar{J}^2)}}{2(M^2 + \bar{\Lambda}\bar{J}^2)} \right]^{1/2}, \quad (61)$$

that corresponds to the minimum radius for this orbit. Note that the above equation diverges at $J = J_{L \rightarrow \infty} = \sqrt{-M^2/\bar{\Lambda}}$. Also, for $J^2 < -M^2/\bar{\Lambda}$, R_U became imaginary. On the other hand, the radius of the last stable circular orbit must satisfied $V'|_{r_{LSCO}, L_{LSCO}} = 0$ and $V''|_{r_{LSCO}, L_{LSCO}} = 0$, and it is given by

$$r_{LSCO} = \left[\frac{L_{LSCO}^2(J^2 - \bar{J}^2)}{4(-\bar{\Lambda})} \right]^{1/6}. \quad (62)$$

Therefore, in the range $J_{L \rightarrow \infty} < J < J_M$ the black hole has two horizons and the effective potential allows circular and planetary orbits for $L > L_{LSCO}$.

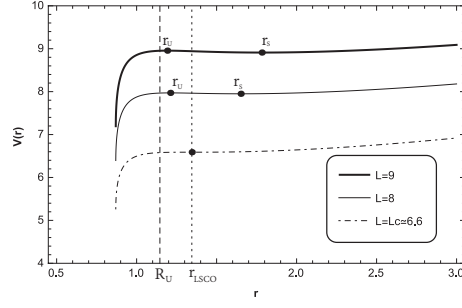


FIG. 10: The behavior of $V(r)$ as a function of r , for different values of the angular momentum of the particle L , with $M = a = b = \lambda = 1$, $\xi = 1.1$, $r_+ \approx 0.87$, $J = 1.2$, $\Lambda = -1$, $R_U = 1.15$ and $r_{LSCO} = 1.34$. For $L = 8$, $r_U = 1.21$, and $r_S = 1.65$. For $L = 9$, $r_U = 1.19$, and $r_S = 1.78$. Here, $L_c = L_{LSCO}$.

Also, it is possible to determine the periods of revolution of the circular orbits, both stable and unstable, with respect to the proper time τ , $T_\tau = 2\pi/\dot{\phi}(r_{c.o.})$, and coordinate time t , $T_t = T_\tau \dot{t}(r_{c.o.})$. Thereby, the period of a revolution according to the proper time is

$$T_\tau = \frac{4\pi(-\bar{\Lambda})r_{c.o.}(r_{c.o.}^2 - r_+^2)(r_{c.o.}^2 - r_-^2)}{J\sqrt{(r_{c.o.}^2 + L_{c.o.}^2)\mathcal{F}(r_{c.o.}) + 2L_{c.o.}r_{c.o.}\mathcal{F}(r_{c.o.})}}, \quad (63)$$

and the period according to the coordinate time is

$$T_t = \frac{4\pi r_{c.o.}^2 \sqrt{(r_{c.o.}^2 + L_{c.o.}^2)\mathcal{F}(r_{c.o.})}}{J\sqrt{(r_{c.o.}^2 + L_{c.o.}^2)\mathcal{F}(r_{c.o.}) + 2L_{c.o.}r_{c.o.}\mathcal{F}(r_{c.o.})}}. \quad (64)$$

On the other hand, Taylor expanding the effective potential around $r = r_S$, one can write $V(r) = V(r_S) + V'(r_S)(r - r_S) + \frac{1}{2}V''(r_S)(r - r_S)^2 + \dots$, where $'$ means derivative with respect to the radial coordinate. Obviously, in these orbits $V'(r_S) = 0$, so, by defining the *smaller* coordinate $x = r - r_S$, together with *the epicycle frequency* $\kappa^2 = V''(r_S)$ [20], we can rewrite the above equation as $V(x) \approx E_S + \kappa^2 x^2/2$ where E_S is the energy of the particle in the stable circular orbit. Also, it is easy to see that test particles satisfy the harmonic equation of motion $\ddot{x} = -\kappa^2 x$. Therefore, the epicycle frequency is given by

$$\kappa^2 = \frac{JL_{c.o.}}{r^4} \left[3 + \frac{r^4 \mathcal{F}'' + r^2 L_{c.o.}^2 \mathcal{F}'' - 4r \mathcal{F}' L_{c.o.}^2 + 6L_{c.o.}^2 \mathcal{F}}{r^3 \mathcal{F}' + r \mathcal{F}' L_{c.o.}^2 - 2L_{c.o.}^2 \mathcal{F}} - \frac{r^3 \mathcal{F}' + r \mathcal{F}' L_{c.o.}^2 - 2L_{c.o.}^2 \mathcal{F}}{2(r^2 \mathcal{F} + L_{c.o.}^2 \mathcal{F})} \right] \Big|_{r_S}. \quad (65)$$

In the case of non-rotating black holes, the polynomial (57) has analytical solution and it at $r = r_{ext}$ can be written as

$$r_{ext}^6 + \frac{1}{\bar{\Lambda}} \left(\frac{\bar{J}^2}{4} - ML^2 \right) r_{ext}^2 + \frac{\bar{J}^2 L^2}{2\bar{\Lambda}} = 0, \quad (66)$$

where the quadratic term is null for $L = L_1 = \frac{\bar{J}}{2\sqrt{M}}$. The root of this polynomial is

$$r_{ext} = \left(\sqrt{\frac{\chi_2}{3}} \cosh \left[\frac{1}{3} \cosh^{-1} \left(3\chi_3 \sqrt{\frac{3}{\chi_2^3}} \right) \right] \right)^{1/2}, \quad (67)$$

for $0 < L < L_1$.

$$r_{ext} = \left(\frac{\bar{J}^2 L_1^2}{-2\bar{\Lambda}} \right)^{1/6} = \left(\frac{\bar{J}^4}{-8M\bar{\Lambda}} \right)^{1/6}, \quad (68)$$

for $L = L_1$, and

$$r_{ext} = \left(\sqrt{\frac{-\chi_2}{3}} \sinh \left[\frac{1}{3} \sinh^{-1} \left(3\chi_3 \sqrt{\frac{3}{-\chi_2^3}} \right) \right] \right)^{1/2}, \quad (69)$$

for $L > L_1$, where

$$\chi_2 = -\frac{4}{\Lambda} \left(\frac{\bar{J}^2}{4} - ML^2 \right), \quad \chi_3 = -\frac{2\bar{J}^2 L^2}{\Lambda}. \quad (70)$$

In Fig. 11 we show the behaviour of the effective potential for non-rotating black holes for large and small values of L , and in Fig. 12, we show that the lapse function at $r = r_{ext}$ is negative for different values of L . Therefore, for

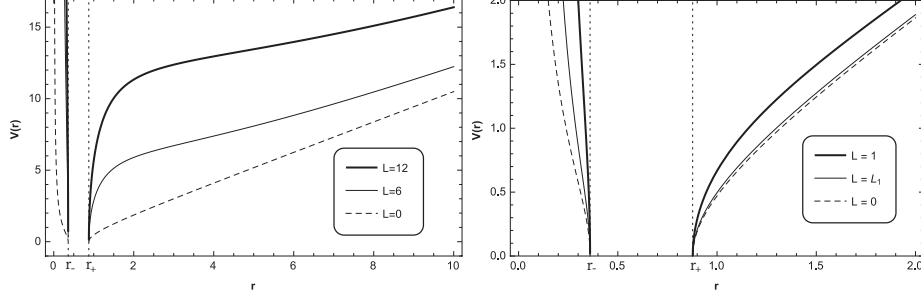


FIG. 11: The behavior of $V(r)$ as a function of r , for different values of the angular momentum of the particle L , with $M = a = b = \lambda = 1$, $J = 0$, $\xi = 0.9$ and $\Lambda = -1$. Here $r_+ = 0.878$, $r_- = 0.360$, and $L_1 = 0.333$.

$J = 0$ we have shown that there are no circular orbits in the domain $r > r_+$.

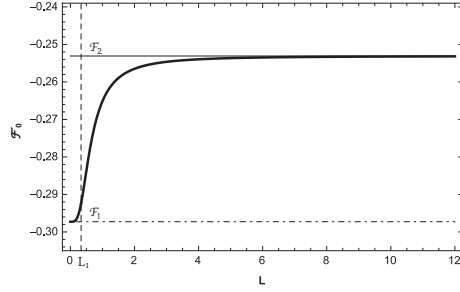


FIG. 12: The behavior of $\mathcal{F}_0(L)$ as a function of L , with $M = a = b = \lambda = 1$, $J = 0$, $\xi = 0.9$, $L_1 = 0.333$, and $\Lambda = -1$. The metric function at $r = r_{ext}$ tends to $\mathcal{F}_2 = -0.253$ when $L \rightarrow \infty$ and it tends to $\mathcal{F}_1 = -0.297$ when $L \rightarrow 0$. Here, the function $\mathcal{F}_0(L) = \mathcal{F}[r_{ext}(L)]$, where $\mathcal{F}_1 = \mathcal{F}_0(L \rightarrow 0) = -M + \bar{J}\sqrt{-\Lambda}$, and $\mathcal{F}_2 = \mathcal{F}_0(L \rightarrow \infty) = -\frac{M}{2} + \frac{\bar{J}^2(-\Lambda)}{2M}$.

On the other hand, in Fig. 13, we show that there is not circular orbit in the relevant domain $r > r_+$, for black holes with one horizon (left panel) and for black holes with an inner and outer horizon (right panel). Moreover, in this domain, the behaviour for a non-rotating black hole is similar to the behaviour for small values of $|J|$.

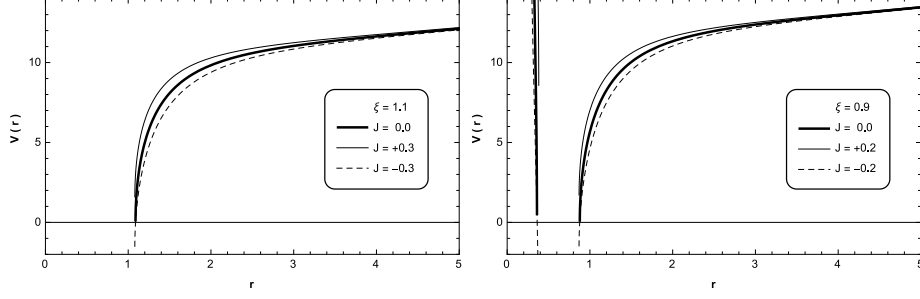


FIG. 13: The behaviour of the effective potential $V(r)$ as a function of r , for different values of the angular momentum of the black hole J , with $M = a = b = \lambda = 1$, $\Lambda = -1$, and $L = 12$. Left panel for $\xi = 1.1$, and right panel for $\xi = 0.9$.

C. Critical trajectories

There are two critical orbits that approach to the unstable circular orbit asymptotically. In the first kind, the particle arises from $r = r_A$, and in the second kind, the particle starts from a finite distance $r = r_i$ bigger than the horizon radius, but smaller than the unstable radius, see Fig. 14. By considering $\phi = t = \tau = 0$, and Eq. (24), the proper time for the critical orbit of first kind is

$$\tau(r) = -\frac{1}{(-\bar{\Lambda})^{1/2}} \int_{r_A}^r \frac{r^2 dr}{(r^2 - r_U^2) \sqrt{r_A^2 - r^2}}, \quad (71)$$

whose solution is given by

$$\tau(r) = \frac{1}{\sqrt{-\bar{\Lambda}}} \left[\psi(r) + \frac{r_U}{\sqrt{r_A^2 - r_U^2}} \psi_U(r) \right], \quad (72)$$

where

$$\psi[r] = \tan^{-1} \sqrt{\frac{r_A^2}{r^2} - 1}, \quad (73)$$

and

$$\psi_U[r] = \tanh^{-1} \left[\frac{r_U}{r} \sqrt{\frac{r_A^2 - r^2}{r_A^2 - r_U^2}} \right]. \quad (74)$$

Now, for the critical trajectories of second kind the proper time is

$$\tau(r) = \frac{1}{\sqrt{-\bar{\Lambda}}} \left[\psi(r) - \psi(r_i) + \frac{r_U [\psi_U(r) - \psi_U(r_i)]}{\sqrt{r_A^2 - r_U^2}} \right], \quad (75)$$

On the other hand, by considering $\phi = t = \tau = 0$, Eqs. (23) and (24) the coordinate time for the critical trajectory of first kind is

$$t(r) = -\int_{r_A}^r \frac{r^2 [Er^2 - JL/2] dr}{(-\bar{\Lambda})^{3/2} (r^2 - r_+^2)(r^2 - r_-^2)(r^2 - r_U^2) \sqrt{r_A^2 - r^2}}, \quad (76)$$

whose solution is

$$t(r) = \frac{1}{(-\bar{\Lambda})^{3/2}} \sum_{j=1}^3 \tilde{k}_j \psi_j(r), \quad (77)$$

where

$$\psi_1(r) = \frac{r_U}{\sqrt{r_A^2 - r_U^2}} \tanh^{-1} \left[\frac{r_U}{r} \sqrt{\frac{r_A^2 - r^2}{r_A^2 - r_U^2}} \right], \quad (78)$$

$$\psi_2(r) = \frac{r_+}{\sqrt{r_A^2 - r_+^2}} \tanh^{-1} \left[\frac{r_+}{r} \sqrt{\frac{r_A^2 - r^2}{r_A^2 - r_+^2}} \right], \quad (79)$$

$$\psi_3(r) = \frac{r_-}{\sqrt{r_A^2 - r_-^2}} \tanh^{-1} \left[\frac{r_-}{r} \sqrt{\frac{r_A^2 - r^2}{r_A^2 - r_-^2}} \right] \quad (80)$$

and

$$\tilde{k}_1 = \frac{Er_U^2 - JL/2}{(r_U^2 - r_+^2)(r_U^2 - r_-^2)}, \quad \tilde{k}_2 = -\frac{Er_+^2 - JL/2}{(r_U^2 - r_+^2)(r_+^2 - r_-^2)}, \quad \tilde{k}_3 = \frac{Er_-^2 - JL/2}{(r_U^2 - r_-^2)(r_+^2 - r_-^2)}. \quad (81)$$

For the critical trajectories of second kind the coordinate time is

$$t(r) = \frac{1}{(-\bar{\Lambda})^{3/2}} \sum_{j=1}^3 \tilde{k}_j [\psi_j(r) - \psi_j(r_i)]. \quad (82)$$

In Fig. 14, we plot the behaviour of the proper and coordinate time as a function of r . We observe that for both times, the particle take an infinity time in to arrive to the unstable circular orbit. Finally, by using Eq. (22), and

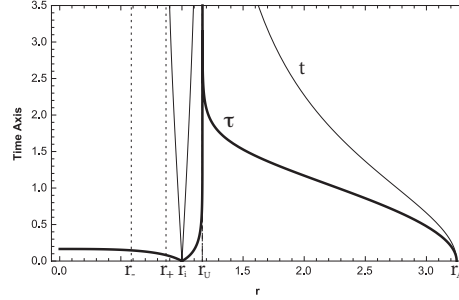


FIG. 14: The behaviour of the proper (τ) (thick line) and coordinate (t) (thin line) time as a function of r for critical trajectories of first and second kind with $M = a = b = \lambda = 1$, $\bar{\Lambda} = -1$, $J = 1.2$, $\xi = 1.1$, $r_- \approx 0.59$, $r_+ \approx 0.87$, $r_i = 1.00$, $r_U \approx 1.17$, $r_A \approx 3.25$, and $E_U \approx 11.92$.

(24), the angular coordinate ϕ for the trajectories of first kind is

$$\phi_C(r) = \frac{1}{(-\bar{\Lambda})^{3/2}} \sum_{i=1}^3 \eta_i \psi_i(r), \quad (83)$$

where

$$\eta_1 = \frac{1}{(r_U^2 - r_+^2)(r_U^2 - r_-^2)} \left(\frac{E_U J}{2} - LM + (-\bar{\Lambda})L r_U^2 - \frac{L(J^2 - \bar{J}^2)}{4r_U^2} \right), \quad (84)$$

$$\eta_2 = \frac{-1}{(r_U^2 - r_+^2)(r_+^2 - r_-^2)} \left(\frac{E_U J}{2} - LM + (-\bar{\Lambda})L r_+^2 - \frac{L(J^2 - \bar{J}^2)}{4r_+^2} \right), \quad (85)$$

$$\eta_3 = \frac{1}{(r_U^2 - r_-^2)(r_+^2 - r_-^2)} \left(\frac{E_U J}{2} - LM + (-\bar{\Lambda})L r_-^2 - \frac{L(J^2 - \bar{J}^2)}{4r_-^2} \right). \quad (86)$$

While that for critical trajectories of second kind is

$$\phi_C(r) = \frac{1}{(-\Lambda)^{3/2}} \sum_{j=1}^3 \eta_j [\psi_j(r) - \psi_j(r_i)] . \quad (87)$$

In Fig. 15, we show the behavior of the angular coordinate as a function of r . We can observe that for both trajectories, first and second kind, the angular coordinate diverges at the unstable circular radius.

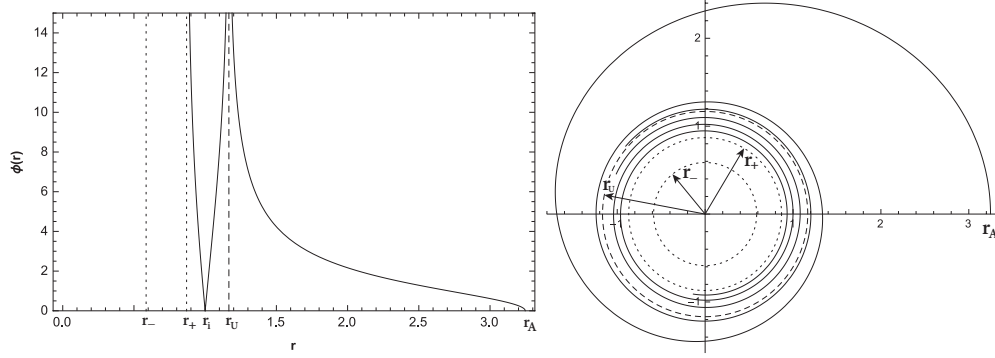


FIG. 15: Critical trajectory of first and second kind, for particles with $L = 12$, $M = a = b = \lambda = 1$, $\Lambda = -1$, $J = 1.2$, $\xi = 1.1$, $E_U = 11.92$, $r_- \approx 0.59$, $r_+ \approx 0.87$, and $r_i = 1.0$. For orbit of the first kind (thin line) the test particle arrived from $r_A = 3.25$, where $r_U \approx 1.17$ corresponds to the radius of the unstable circular orbit (dashed circle).

D. Motion with $L = 0$

In this case, the particles are destined to fall towards the event horizon, see Fig. 5. The effective potential Eq. (25) is $V(r) = \left(-M + \frac{\bar{J}^2}{4r^2} - \bar{\Lambda}r^2\right)^{1/2}$, and Eqs. (22), (23) and (24) yield

$$\dot{\phi} = -\frac{E J}{2\bar{\Lambda}(r^2 - r_+^2)(r^2 - r_-^2)}, \quad (88)$$

$$\dot{t} = -\frac{E r^2}{\bar{\Lambda}(r^2 - r_+^2)(r^2 - r_-^2)}, \quad (89)$$

$$\pm \dot{r} = \sqrt{E^2 + M - \frac{\bar{J}^2}{2r^2} + \bar{\Lambda}r^2}, \quad (90)$$

where the $(-)$ sign for \dot{r} , corresponds to particles falling into the event horizon, and the $(+)$ sign corresponds to particles that have a return point $r_0 > r_+$, for $E > E_+$, given by

$$r_0 = \sqrt{\frac{M + E^2}{-\bar{\Lambda}}} \sin \left[\frac{1}{2} \sin^{-1} \left(\frac{\bar{J}\sqrt{-\bar{\Lambda}}}{M + E^2} \right) + \frac{\pi}{2} \right], \quad (91)$$

and a return point at $d_0 < r_-$, given by

$$d_0 = \sqrt{\frac{M + E^2}{-\bar{\Lambda}}} \sin \left[\frac{1}{2} \sin^{-1} \left(\frac{\bar{J}\sqrt{-\bar{\Lambda}}}{M + E^2} \right) \right]. \quad (92)$$

Now, choosing as initial conditions that the particle starts at $r = r_0$, and $\phi = t = \tau = 0$, the solution of Eq. (90) is

$$\tau(r) = \frac{1}{2\sqrt{-\bar{\Lambda}}} \left(\sin^{-1} \left[\frac{M + 2\bar{\Lambda}r^2 + E^2}{\sqrt{\bar{J}^2\bar{\Lambda} + (M + E^2)^2}} \right] - \sin^{-1} \left[\frac{M + 2\bar{\Lambda}r_0^2 + E^2}{\sqrt{\bar{J}^2\bar{\Lambda} + (M + E^2)^2}} \right] \right). \quad (93)$$

Also, a straightforward integration of Eqs. (89) and (90) leads to

$$t(r) = \frac{E}{2(-\bar{\Lambda})^{3/2}} \left[\frac{r_+^2}{\sqrt{p(r_+)}} \ln \left| \frac{r_0^2 - r_+^2}{r^2 - r_+^2} \cdot \frac{F_+(r)}{F_+(r_0)} \right| - \frac{r_-^2}{\sqrt{p(r_-)}} \ln \left| \frac{r_0^2 - r_-^2}{r^2 - r_-^2} \cdot \frac{F_-(r)}{F_-(r_0)} \right| \right], \quad (94)$$

where

$$F_{\pm}(r) = 2p(r_{\pm}) + \left(\frac{E^2 + M}{-\bar{\Lambda}} - 2r_{\pm}^2 \right) (r^2 - r_{\pm}^2) + 2\sqrt{p(r_{\pm})}\sqrt{P_{\pm}(r)}, \quad (95)$$

$$p(r) = -r^4 + \frac{E^2 + M}{-\bar{\Lambda}}r^2 - \frac{\bar{J}^2}{4(-\bar{\Lambda})}, \quad (96)$$

$$P_{\pm}(r) = p(r_{\pm}) + \left(\frac{E^2 + M}{-\bar{\Lambda}} - 2r_{\pm}^2 \right) (r^2 - r_{\pm}^2) - (r^2 - r_{\pm}^2)^2. \quad (97)$$

In Fig. 16, we show the behaviour of the proper and coordinate time as a function of r , we can observe that the particle arrives to the event horizon in a finite proper time, then the particle does not reach the singularity, due to the existence of a return point d_0 inside r_- , see Fig. 4. Concerning to the coordinate time, the particle arrives in an infinite coordinate time to the singularity. Finally, the solution for the angular coordinate ϕ is

$$\phi(r) = \frac{E J}{4(-\bar{\Lambda})^{3/2}} \left[\frac{1}{\sqrt{p(r_+)}} \ln \left| \frac{r_0^2 - r_+^2}{r^2 - r_+^2} \cdot \frac{F_+(r)}{F_+(r_0)} \right| - \frac{1}{\sqrt{p(r_-)}} \ln \left| \frac{r_0^2 - r_-^2}{r^2 - r_-^2} \cdot \frac{F_-(r)}{F_-(r_0)} \right| \right], \quad (98)$$

where we have used Eq. (88) and Eq. (90). In Fig. 17, we plot the behaviour of the angular coordinate, where we observe that the angular coordinate becomes infinity at the event horizon.

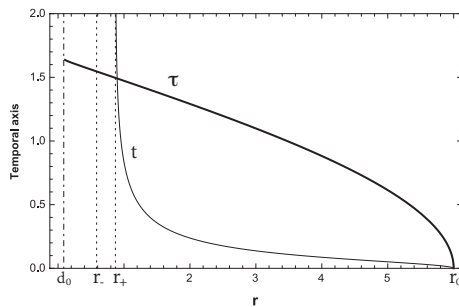


FIG. 16: The behaviour of the coordinate time (t) and the proper time (τ) along an unbounded time-like radial geodesic described by a test particle, starting at $r_0 = 6$ and falling towards the singularity, for $L = 0$, $M = a = b = \lambda = 1$, $\Lambda = -1$, $E = 5.63$, $J = 1.2$, $\xi = 1.1$, $r_+ \approx 0.87$, $d_0 = 0.085$, and $r_- \approx 0.59$.

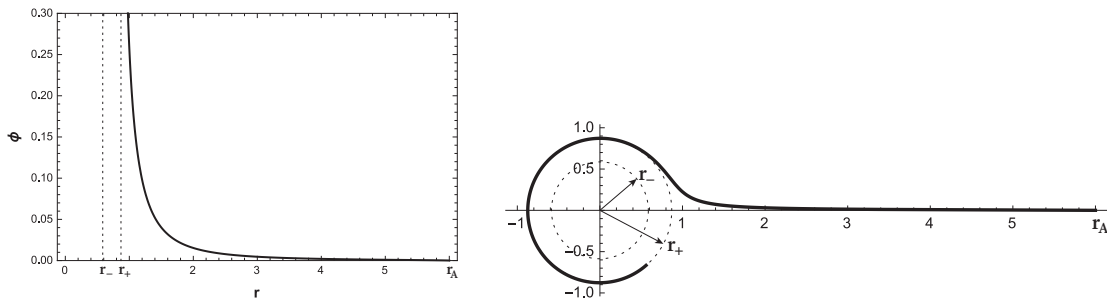


FIG. 17: The behavior of the coordinate $\phi(r)$, starting at $r_0 = 6$ and falling towards the singularity with $L = 0$, $M = a = b = \lambda = 1$, $\Lambda = -1$, $J = 1.2$, $\xi = 1.1$, $r_- \approx 0.59$ and $r_+ = 0.87$. In the polar plot, the trajectory approaching the horizon will spiral around the black hole an infinite number of times.

V. REMARKS AND CONCLUSIONS

In this work, we studied the motion of particles in the background of a rotating three-dimensional Hořava AdS black hole described by a Lorentz-violating version of the BTZ black hole, and we calculated the time like geodesics, which possess a rich structure and allow different kinds of trajectories for the particles. This work along with the null geodesic described in Ref. [10], complements the geodesic structure for the rotating three-dimensional Hořava AdS black hole. For direct orbits, we have shown the existence of planetary orbits, where we have obtained an exact solution and we have determined the periods of revolution. Also, for circular orbits, we have shown the existence of the stable and unstable circular orbits, and we determined the periods of revolution, as well as, the epicycle frequency for the stable circular orbit. Also, critical orbits of first and second kind that approach to the unstable circular orbit asymptotically. For the motion with $0 \leq L < L_C$, the trajectories are all bounded, and for $L = 0$, we have obtained exact solutions. However, their counterpart, i.e., the BTZ metric allows geodesics for massive particles that always fall into the event horizon and no stable orbits are possible; thereby, the differences observed with respect to the BTZ metric could be attributed to the breaking of the Lorentz invariance. On the other hand, for retrograde orbits we have shown the existence of second kind orbits, similar to the behaviour observed for retrograde orbits in a BTZ black hole background [4]. In addition, by comparing both orbits, direct and retrograde, in a rotating three-dimensional Hořava AdS black hole it is possible to observe trajectories with $E \leq 0$ for retrograde orbits which is not possible for direct orbits.

Therefore, the Lorentz-violating version of the BTZ black hole, turns on an effective potential with a more rich structure allowing different kinds of orbits. As it was shown [10], for photons new kinds of orbits are allowed, such as unstable circular orbits and trajectories of first kind. While that for particles the planetary and circular orbits are allowed, which does not occur in the BTZ background. In this way, the breaking of the Lorentz invariance could generate orbits that could not occur in invariant Lorentz theories.

Acknowledgments

We thank the referee for his/her careful review of the manuscript and his/her valuable comments and suggestions which helped us to improve the manuscript. Y.V. acknowledge support by the Dirección de Investigación y Desarrollo de la Universidad de La Serena, Grant No. PR18142.

-
- [1] M. Banados, C. Teitelboim and J. Zanelli, “The Black hole in three-dimensional space-time,” *Phys. Rev. Lett.* **69** (1992) 1849 [hep-th/9204099].
 - [2] S. Carlip, “The (2+1)-Dimensional black hole,” *Class. Quant. Grav.* **12**, 2853 (1995) [gr-qc/9506079].
 - [3] C. Farina, J. Gamboa and A. J. Segui-Santonja, “Motion and trajectories of particles around three-dimensional black holes,” *Class. Quant. Grav.* **10**, L193 (1993) [gr-qc/9303005].
 - [4] N. Cruz, C. Martinez and L. Pena, “Geodesic structure of the (2+1) black hole,” *Class. Quant. Grav.* **11**, 2731 (1994) [gr-qc/9401025].
 - [5] T. P. Sotiriou, M. Visser and S. Weinfurtner, “Lower-dimensional Horava-Lifshitz gravity,” *Phys. Rev. D* **83**, 124021 (2011) [arXiv:1103.3013 [hep-th]].
 - [6] T. P. Sotiriou, I. Vega and D. Vernieri, “Rotating black holes in three-dimensional Hořava gravity,” *Phys. Rev. D* **90**, no. 4, 044046 (2014) [arXiv:1405.3715 [gr-qc]].
 - [7] P. Horava, “Quantum Gravity at a Lifshitz Point,” *Phys. Rev. D* **79**, 084008 (2009) [arXiv:0901.3775 [hep-th]].
 - [8] R. Bécar, P. A. González, E. Papantonopoulos and Y. Vásquez, “Quasinormal modes of three-dimensional rotating Hořava AdS black hole and the approach to thermal equilibrium,” *Eur. Phys. J. C* **80**, no. 7, 600 (2020) [arXiv:1906.06654 [gr-qc]].
 - [9] R. Bécar, P. A. González and Y. Vásquez, “Collision of particles near a three-dimensional rotating Hořava AdS black hole,” arXiv:2002.04421 [gr-qc].
 - [10] P. A. González, M. Olivares, E. Papantonopoulos and Y. Vásquez, “Motion and trajectories of photons in a three-dimensional rotating Hořava-AdS black hole,” *Phys. Rev. D* **101**, no. 4, 044018 (2020) [arXiv:1912.00946 [gr-qc]].
 - [11] S. Fernando, D. Krug and C. Curry, “Geodesic structure of static charged black hole solutions in 2+1 dimensions,” *Gen. Rel. Grav.* **35**, 1243 (2003).
 - [12] N. Cruz, M. Olivares and J. R. Villanueva, “Geodesic Structure of Lifshitz Black Holes in 2+1 Dimensions,” *Eur. Phys. J. C* **73**, 2485 (2013) [arXiv:1305.2133 [gr-qc]].
 - [13] S. Kazempour and S. Soroushfar, “Investigation the geodesic motion of three dimensional rotating black holes,” *Chin. J. Phys.* **65**, 579 (2020) [arXiv:1709.06541 [gr-qc]].
 - [14] G. Panotopoulos, “Orbits of test particles in three-dimensional Maxwell–Dilaton spacetime: exact analytical solution to the geodesic equation,” *Gen. Rel. Grav.* **52**, no. 6, 54 (2020).
 - [15] T. Jacobson, “Extended Horava gravity and Einstein-aether theory,” *Phys. Rev. D* **81**, 101502 (2010) Erratum: [*Phys. Rev. D* **82**, 129901 (2010)] [arXiv:1001.4823 [hep-th]].
 - [16] B. Cropp, S. Liberati, A. Mohd and M. Visser, “Ray tracing Einstein-Æther black holes: Universal versus Killing horizons,” *Phys. Rev. D* **89**, no. 6, 064061 (2014) [arXiv:1312.0405 [gr-qc]].
 - [17] T. Zhu, Q. Wu, M. Jamil and K. Jusufi, “Shadows and deflection angle of charged and slowly rotating black holes in Einstein-Æther theory,” *Phys. Rev. D* **100**, no. 4, 044055 (2019)
 - [18] Chandrasekhar S.: *The Mathematical Theory of Black Holes*. Oxford University Press, New York (1983).
 - [19] N. Deruelle and R. Ruffini, “Quantum and classical relativistic energy states in stationary geometries,” *Phys. Lett.* **52B**, 437 (1974).
 - [20] J. Ramos-Caro, J. F. Pedraza and P. S. Letelier, “Motion around a Monopole + Ring system: I. Stability of Equatorial Circular Orbits vs Regularity of Three-dimensional Motion,” *Mon. Not. Roy. Astron. Soc.* **414**, 3105 (2011) [arXiv:1103.4616 [astro-ph.EP]].
 - [21] In this work, we have considered a choosing of values for the parameters such that the zeros of term in square-brackets are not located in the relevant domain they are inside the event horizon.